Influence of Bone Volume Fraction and Architecture on Computed Large-Deformation Failure Mechanisms in Human Trabecular Bone

Grant Bevill[1,2]
Senthil K Eswaran[1,2]
Atul Gupta[1]
Panayiotis Papadopoulos[2,4]
Tony M. Keaveny[1,2,3]

[1]Orthopaedic Biomechanics Laboratory, University of California, Berkeley, CA, USA
[2]Department of Mechanical Engineering, University of California, Berkeley, CA, USA
[3]Department of Bioengineering, University of California, Berkeley, CA, USA
[4]Computational Solid Mechanics Laboratory, University of California, Berkeley, CA, USA

Corresponding author:
Grant Bevill
2166 Etcheverry Hall
University of California
Berkeley, CA 94720-1740
USA
(510) 642-3787, fax (510) 642-6163
gbevill@me.berkeley.edu

Please address all reprint requests to:
Tony M. Keaveny
6175 Etcheverry Hall
University of California
Berkeley, CA 94720-1740
USA
(510) 643-8017, fax (510) 642-6163
tmk@me.berkeley.edu

Key words

cancellous bone

finite element modeling

biomechanics

bone strength

finite deformation

Abstract

Large-deformation bending and buckling have long been proposed as failure mechanisms by which the strength of trabecular bone can be affected disproportionately to changes in bone density, and thus may represent an important aspect of bone quality. We sought here to quantify the contribution of large-deformation failure mechanisms on strength, to determine the dependence of these effects on bone volume fraction and architecture, and to confirm that the inclusion of large-deformation effects in high-resolution finite element models improves predictions of strength versus experiment. Micro-CT-based finite element models having uniform hard tissue material properties were created from 54 cores of human trabecular bone taken from four anatomic sites (age = 70 ± 11; 24 male, 27 female donors), which were subsequently biomechanically tested to failure. Strength predictions were made from the models first including, then excluding, large-deformation failure mechanisms, both for compressive and tensile load cases. As expected, strength predictions versus experimental data for the large deformation finite element models were significantly improved ($p < 0.001$) relative to the small deformation models in both tension and compression. Below a volume fraction of about 0.20, large-deformation failure mechanisms decreased trabecular strength from 5-80% for compressive loading, while effects were negligible above this volume fraction. Step-wise nonlinear multiple regression revealed that structure model index (SMI) and volume fraction (BV/TV) were significant predictors of these reductions in strength ($R^2 = 0.83$, $p < 0.03$). Even so, some low-density specimens having nearly identical volume fraction and SMI exhibited up to five fold differences in strength reduction. We conclude that within very low-density bone, the potentially important biomechanical effect of

large-deformation failure mechanisms on trabecular bone strength is highly heterogeneous and is not well explained by standard architectural metrics.

Introduction

In the context of osteoporotic and anti-resorptive drug-treated bone, recent studies have shown that DXA cannot fully explain decreases in fracture risk associated with increases in areal bone mineral density [1, 2]. Accordingly, it has been proposed that bone quality effects, such as trabecular architecture, have an independent contribution to fracture risk [3, 4], whereby factors such as excessive trabecular thinning or loss of connectivity are thought to predispose trabeculae to fail by mechanisms such as large-deformation bending or buckling [5, 6]. Quantification of the effect of these types of failure mechanisms on trabecular strength and relating them to architecture — a potentially important aspect of bone quality — should provide insight into the etiology of osteoporotic fracture and the mechanisms by which drug treatments reduce fracture risk.

Because of the great technical difficulty of directly observing the failure mechanisms within trabecular bone in real time, much of the existing information on trabecular failure mechanisms comes from computational and theoretical studies. Cellular solid theory predicts that high-density trabecular bone likely fails by tissue-level yielding [7], and that low-density bone likely fails by excessive bending [8] or buckling [7], consistent with the form of strength-density characteristics observed in experimental studies [9, 10]. Even greater detail on tissue-level trabecular failure mechanisms can be obtained from high-resolution finite element models [11-13]. However, geometrically nonlinear finite element analysis must be performed in order to describe certain failure mechanisms—namely, large-deformation bending and buckling [14]. Previous high-resolution finite element studies derived from micro-CT scans have already shown that large-deformation effects may be significant even at the yield point [11, 14, 15], an initial

indicator of failure which occurs well before trabeculae fracture [16, 17]. Other evidence suggests that the effects of large-deformation failure mechanisms on trabecular strength should be negligible in very high-density bone [7, 9, 11, 12, 18]. However, the effects of large-deformation failure mechanisms on strength in intermediate and low-density bone are not clear, nor their dependence on architecture and bone volume fraction [19].

Using state-of-the-art developments in high-resolution finite element analysis in conjunction with biomechanical testing, we sought to understand the effects of large-deformation failure mechanisms on trabecular bone strength. We used trabecular bone from a variety of anatomic sites displaying large differences in bone volume fraction and architecture. Our specific objectives were to: 1) quantify the independent contribution of large-deformation failure mechanisms to trabecular bone strength as a function of architecture and bone volume fraction; 2) determine the volume fraction below which the effect of large-deformation mechanisms on strength becomes appreciable; and 3) confirm that the incorporation of large deformations improves finite element predictions versus experimental measurements of trabecular strength. By using computer models based solely on the trabecular architecture to extract the independent role of large deformation failure mechanisms on trabecular bone strength, this analysis provides unique insight into bone quality issues associated with trabecular architecture.

Methods

Fifty-four cylindrical (8 mm diameter, 20 mm length), cadaveric specimens of trabecular bone were selected from the human femoral neck (n=21), greater trochanter (n=7), proximal tibia (n=7), and vertebral body (n=19) (Table 1). All specimens were

prepared such that the main trabecular orientation was aligned with the axis of the core [20]. None of the donors had a history of metabolic bone disease or cancer and all specimens showed no radiographic evidence of damage or bone pathologies. Three-dimensional high-resolution images were obtained of the full cylindrical core for each specimen using micro-CT (Scanco μCT 20; Scanco Medical AG, Basserdorf, Switzerland) or serial milling [21]. Images were then coarsened using region-averaging to either 40 or 60 μm spatial resolution such that the size of the resulting finite elements was less than one-fourth of the mean trabecular thickness. Such element sizes are recommended for use in elastic analyses [22], and we confirmed numerical convergence for our fully non-linear models (Appendix A). The grayscale images were thresholded such that the volume fraction matched the experimentally measured value. A finite element model was obtained from each scan by converting individual voxels into eight-noded brick elements [23]. Individual models had up to 2.7 million elements.

The same finite plasticity material model [24, 25] was used to model the trabecular tissue in all finite element analyses. The elasto-plasticity model is of the rate-independent type described by the theory of Green and Naghdi [26, 27], and was proposed for the modeling of solids that exhibit elastic-plastic type stress-strain behavior at the macroscopic scale. Linear isotropic hardening was incorporated in the model, and kinematic hardening was defined by a rate-type constitutive law. Tension-compression asymmetry in trabecular tissue yield strength was also included via pseudo-kinematic hardening. A Poisson's ratio of 0.3 and a specimen-specific isotropic modulus was used to model the hard tissue, for which the tissue modulus was determined using a combined computational-experimental technique [13, 28]. The tissue-level yield strains in tension

(0.33%) and compression (0.81%) were calibrated for 12 of the femoral neck specimens following an iterative algorithm [29].

Using the above nonlinear material model for all subsequent analyses, small-deformation (geometrically linear) and then large-deformation (geometrically nonlinear) finite element analyses were performed for each of the 54 models, and this was done for both apparent tensile and compressive loading (216 analyses in total). This approach eliminated any possible confounding effects of tissue mineralization on the outcome variables, resulting in effects that were due solely to the volume fraction and architecture of the trabecular structure. A highly scalable, implicit parallel finite element framework (Olympus, [30]) was used for all finite element analyses, performed on a Cray-Dell PowerEdge Xeon cluster parallel supercomputer (Dell, Round Rock, Texas). Total CPU time was approximately 34,320 hours, equivalent to about 613 hours in real time since typically 56 CPUs were used in parallel for each analysis.

The apparent yield point was determined from the apparent stress-strain curve of each specimen using the 0.2% offset method, the elastic modulus being obtained from the first step of the analysis. Our main outcome parameter was the percent change in strength due to the inclusion/exclusion of the large-deformation failure mechanisms within the model (Fig. 1). Using this parameter, the minimum bone volume fraction above which the percent change in strength was less than 5% across all specimens was then determined for both compressive and tensile loading. We termed these the "critical" values of bone volume fraction.

To elucidate the mechanisms of large-deformation failure, multivariate regression and partial correlation analyses (JMP, Version 5.0, SAS Institute Inc., Cary, NC) were

performed on the percent changes in compressive yield strength versus the following micro-architectural measures (Scanco; Scanco Medical AG, Basserdorf, Switzerland) in which the statistical analyses were performed both with and without bone volume fraction: mean trabecular separation (Tb.Sp*), mean trabecular thickness (Tb.Th*), mean trabecular number (Tb.N*), degree of anisotropy (DA), connectivity density (CD) [31], and structure model index (SMI) [32].

To assess whether the inclusion of large deformations improved the accuracy of the models and to establish model validity, finite element predictions of apparent yield stress from both the small- and large-deformation analyses were compared against the corresponding experimental results for both tensile and compressive apparent loading. First, finite element predictions of yield stress were plotted against the experimentally measured values for all specimens in their respective loading modes. Next, in order to gain more insight into role of large-deformation failure mechanisms on the strength predictions for low-density bone, the same variables were re-plotted for only the subset of specimens with bone volume fraction less than the critical values. The error in the finite element predictions of strength were assessed using a single-group t-test to determine if the error was statistically different from zero as well as a paired t-test (JMP, Version 5.0, SAS Institute Inc., Cary, NC) to determine if there was a difference between the predictions from the small- and large-deformation models. This procedure was also repeated for the error in the prediction of yield strain for each specimen, since yield strain represents a more rigorous statistical test than yield stress, given the wide variation in yield stress typically seen across specimens [20].

Details of the mechanical tests are described elsewhere [20]. Briefly, these tests were conducted using a servohydraulic load frame (858 Mini-Bionix, MTS, Eden Prairie, MN) using protocols to minimize the end-artifact effects [10]. Specimens were preconditioned to 0.1% strain, followed by destructive loading to 1.0% strain at 0.5% strain per second. Modulus was determined as the slope at 0% strain of a quadratic curve fit to the portion of the stress-strain curve from 0 to 0.2% strain, and yield was determined using the 0.2% offset technique [20]. In total, 22 specimens were experimentally tested in compression and 32 in tension.

Results

For compressive loading, the reduction in predicted strength due to the inclusion of large-deformation failure mechanisms was always less than 5% for bone having a bone volume fraction greater than 0.20 (Fig. 2A), but was up to 80% for bone below this volume fraction. Since all data points fit on a single exponential relation versus volume fraction, there were no obvious independent effects of anatomic site on the trends. For tensile loading, inclusion of large-deformation failure mechanisms generally resulted in an increase in strength, but the magnitude of the effect was less pronounced than for compressive loading. The increase in strength due to large-deformation failure mechanisms was about 5–30% for bone below a volume fraction of 0.15, and was negligible above this volume fraction (Fig. 2B).

All architectural variables were nonlinearly related to the change in strength due to the inclusion of large-deformation failure mechanisms. After applying a logarithmic-transformation to percent changes in strength, SMI emerged as the best individual

predictor, accounting for 77% ($p < 0.0001$) of the variance (Fig. 3). The step-wise multiple regression model that excluded bone volume fraction ($R^2 = 0.83$) indicated that SMI and Tb.Th* were highly significant predictors of percent change in strength ($p < 0.0001$ and $p = 0.005$, respectively) and CD was marginally significant ($p = 0.01$). When bone volume fraction was included as a variate in the step-wise regression model ($R^2 = 0.82$), SMI remained as the only other significant predictor ($p < 0.03$) beyond bone volume fraction.

The finite element models having large-deformation failure mechanisms were capable of prospectively predicting the yield properties for trabecular bone from both low- and high-density anatomic sites on a specimen-specific basis, whereas the models without large-deformation failure mechanisms only predicted correct behavior for high volume fraction specimens. Across the full range of volume fractions, linear regression analysis showed that both the small- and large-deformation finite element models were able to accurately predict yield stress for compressive and tensile apparent loading equally well (Fig. 4). However, comparison of the error between predicted yield and the corresponding experimental data (i.e., error relative to the ideal line Y=X, Fig. 4) revealed that inclusion of large-deformation failure mechanisms reduced the magnitude of the mean error in the finite element predictions for all cases ($p< 0.0008$, Fig. 5). For the complete data set, errors in yield stress predictions for the large deformation models were statistically indistinguishable from zero ($p > 0.12$) in both loading modes. By contrast, the models without large-deformation failure mechanisms significantly over-predicted yield stress in compression ($p = 0.006$, Fig. 5A) and moderately under-predicted in tension. Similar trends were observed for predictions of yield stress for the

subset of specimens below the critical volume fractions (Fig. 5B), and for predictions of yield strain (Fig. 5C).

Discussion

The results of this study show that large-deformation failure mechanisms can appreciably reduce the strength of trabecular bone, but that this phenomenon depends very much on the volume fraction of the specimen. As expected, inclusion of large-deformation effects brought the finite element model predictions of strength into better agreement with experimental measurements for low-density bone, providing support for the validity of our numerical model. We found that the magnitude of the strength reduction correlated with architectural metrics — primarily the structure model index, mean trabecular thickness, and connectivity density – demonstrating that the large-deformation failure mechanisms were mediated by the transition from plate-like to rod-like structure in trabeculae in conjunction with trabecular thinning and loss of connectivity. However, these standard architectural metrics failed to explain the great heterogeneity in the strength reduction due to large-deformation failure mechanisms observed for specimens having low values of bone volume fraction. Since the computer models used here only included variations in volume fraction and architecture between specimens, our results indicate that there exists a unique bone quality effect related to architecture that can be very large in low-density bone. At present, since standard measures of architecture cannot predict the biomechanical effects of such large-deformation failure mechanisms with much precision, use of fully nonlinear finite

element analysis on micro-CT scans of trabecular bone may provide unique insight into bone quality effects.

The main novelty of this study was the application of fully nonlinear, high-resolution finite element modeling to a large sample size of human trabecular bone taken from a range of anatomic sites that displayed wide variations in architecture and volume fraction. Full cylindrical specimens (8 mm diameter, 20 mm long) were used since our preliminary analyses on 5 mm cubic specimens showed that large-deformation failure mechanisms were artificially attenuated for these smaller specimens, presumably due to constraining effects from the application of roller-type boundary conditions on the top and bottom surfaces of such small specimens (data not shown). While we coarsened our models to resolutions of 40-60 μm, we verified that these resolutions can accurately reproduce yield strength relative to 20 μm models (Appendix A), consistent with recommendations developed previously for prediction of elastic properties [22]. As a further level of validation that our models captured the physical mechanisms initiating yield, we also confirmed the ability of the finite element models to predict the experimentally-observed yield values for the very same 54 specimens simulated here loaded in either tension or compression. While some previous studies have pointed out the importance of geometric nonlinearities in finite element analysis of trabecular bone [11, 14, 15, 18], the possible dependence of large-deformation effects on bone volume fraction, trabecular architecture, and anatomic site has not previously been reported. Advances in computational resources and highly scalable parallel finite element code [30] enabled us to process a large number of specimens efficiently, although it is

expected that such analyses will soon become more routine as computational resources continue to expand.

Despite the overall strengths of the techniques used in this study, certain limitations should also be noted. Our method for isolating failure mechanisms associated with large deformations was purely computational since this would be impossible to do experimentally. Accordingly, the accuracy of our results depends on the fidelity of the models used. Foremost, all finite element analyses assumed homogenous tissue material properties in order to isolate the effects of bone architecture and volume fraction on large-deformation failure mechanisms. However, it has been shown that naturally occurring variations in human trabecular tissue mineralization have only a modest influence on apparent-level elastic properties [33, 34], and it remains as an open question whether these variations affect apparent behavior in the context on nonlinear finite element analysis. For example, the ability of a strain field to localize in nonlinear finite element models provides a means by which the apparent level behavior may become more dependent on local material and geometric details, and remains a topic of ongoing research. Our assumed constitutive model may also represent a limitation of our finite element modeling. First, the material failure rule used in this study is deviatoric-based and assumes that the tissue behaves plastically after yield. Such a model phenomenologically describes the monotonic stress-strain behavior of bone tissue, and was shown to correspond well with experimental strength measurements. Even so, the absolute predictions of the effect of large-deformation failure mechanisms on strength may well depend on the nature of the assumed material failure rule [13]. Second, the hard tissue model used in this study did not include damage or fracture behavior. The

lack of observed micro-fracture of trabeculae at the apparent yield point [16, 17] suggests that modeling of such behavior should not be important in our models, although tissue-level failure and fracture may become increasingly important as the structure is loaded beyond the ultimate point. Our focus here was on effects more relevant to initial failure of trabecular bone and not those associated with catastrophic collapse. Since the ultimate and yield strengths for low-density trabecular bone are highly correlated [35], those architectural factors reported here that affect yield failure will also correlate with ultimate failure. Lastly, the influence of large-deformation failure mechanisms reported here may not be representative of the trabecular bone's *in situ* behavior since we used excised cylindrical specimens for our finite element analyses. Since an interruption in connectivity occurs at the sides of excised specimens of trabecular bone which can appreciably affect apparent-level behavior [36], large-deformation failure mechanisms may occur preferentially in peripheral trabeculae in these specimens. As such, our results may likely provide an upper bound for the effect of large-deformation failure mechanisms on strength with regards to *in situ* behavior.

In addition to the experimental validation of the finite element modeling techniques used in this study, findings from previous experimental [10] and analytical [7, 10] studies also provide support for our estimate of the critical volume fraction at which large-deformation failure mechanisms become appreciable. Both literature studies concluded (in the context of elastic buckling) that large deformations should become appreciable below a volume fraction of about 0.2 for compressive apparent loading. Furthermore, the theoretical transition between deformation mechanisms for trabecular bone when treated as a cellular solid [7] is governed by the change in architecture of the

bone from closed-cell plate-like structure to an open-cell rod-like structure, and is only indirectly related to volume fraction — consistent with our finding that large-deformation effects were best correlated with SMI.

The results from this study help clarify some concerns regarding high-resolution finite element modeling of trabecular bone yield behavior. With the incorporation of a nonlinear material model, small-deformation finite element analyses have been shown to accurately capture the yield behavior of trabecular bone from high-density anatomic sites [11, 12] and have been used in purely computational studies of high-density trabecular bone failure [18, 37]. The results of the present study confirm the validity of this previous work since the small-deformation assumption appears to be appropriate for high-density trabecular bone (above a volume fraction of about 0.2 for compressive loading). The small-deformation assumption can, however, lead to significant errors on a specimen-specific basis for low-density specimens. Even so, we found that the small-deformation finite element models were successful at predicting experimental measures of yield strength across specimens via a linear regression. As such, the need to include the physics of large deformations depends on a study's objectives and may not be necessary in some instances.

Our results have clinical implications regarding changes in the dominant failure mechanisms that may occur with aging, disease, and drug treatment. For example, as evidenced by the heterogeneity in strength reduction due to large-deformation failure mechanisms, it could be that some individuals are more susceptible to these types of failure mechanisms. Since we found that large-deformation failure mechanisms can appreciably decrease bone strength beyond the predictions from bone volume fraction or

standard architectural metrics, clinical assessment of fracture risk or treatment response may be improved by using a combination of non-invasive high-resolution imaging and finite element modeling. Further success at explaining why some low-density specimens are so prone to large-deformation failure mechanisms may provide unique insight into the biomechanical effects of aging, disease, and treatment on trabecular strength.

Acknowledgements

This study was supported by grants from the National Institutes of Health (NIH AR43784) and the National Partnership for Advanced Computational Infrastructure (NPACI UCB254 and UCB266). Dr. Keaveny has a financial interest in O.N. Diagnostics and both he and the company may benefit from the results of this research.

References

1. Delmas, P.D. and E. Seeman, *Changes in bone mineral density explain little of the reduction in vertebral or nonvertebral fracture risk with anti-resorptive therapy*. Bone, 2004. **34**(4): p. 599-604.
2. Cummings, S.R., D.B. Karpf, F. Harris, H.K. Genant, K. Ensrud, A.Z. LaCroix, and D.M. Black, *Improvement in spine bone density and reduction in risk of vertebral fractures during treatment with antiresorptive drugs*. American Journal of Medicine, 2002. **112**(4): p. 281-289.
3. Riggs, B.L. and L.J. Melton, 3rd, *Bone turnover matters: the raloxifene treatment paradox of dramatic decreases in vertebral fractures without commensurate increases in bone density*. J Bone Miner Res, 2002. **17**(1): p. 11-4.
4. Heaney, R.P., *Is the paradigm shifting?* Bone, 2003. **33**(4): p. 457-65.
5. Bell, G.H., O. Dunbar, J.S. Beck, and A. Gibb, *Variations in strength of vertebrae with age and their relation to osteoporosis*. Calcified Tissue Research, 1967. **1**(1): p. 75-86.
6. Snyder, B.D., S. Piazza, W.T. Edwards, and W.C. Hayes, *Role of trabecular morphology in the etiology of age-related vertebral fractures*. Calcified Tissue International, 1993. **53S**(1): p. S14-S22.
7. Gibson, L.J., *The mechanical behavior of cancellous bone*. Journal of Biomechanics, 1985. **18**(5): p. 317-328.
8. Keaveny, T.M., *Strength of trabecular bone*, in *Bone mechanics handbook*, S.C. Cowin, Editor. 2001, CRC press: Boc Raton, Fl. p. **16**-1-42.
9. Müller, R., S.C. Gerber, and W.C. Hayes, *Micro-compression: a novel technique for the nondestructive assessment of local bone failure*. Technology and Health Care, 1998. **6**(5-6): p. 433-44.
10. Kopperdahl, D.L. and T.M. Keaveny, *Yield strain behavior of trabecular bone*. Journal of Biomechanics, 1998. **31**(7): p. 601-8.
11. Morgan, E.F., H.H. Bayraktar, O.C. Yeh, and T.M. Keaveny, *Contribution of inter-site variations in architecture to trabecular bone apparent yield strain*. Journal of Biomechanics, 2003. **37**(9): p. 1413-1420.
12. Niebur, G.L., M.J. Feldstein, J.C. Yuen, T.J. Chen, and T.M. Keaveny, *High-resolution finite element models with tissue strength asymmetry accurately predict failure of trabecular bone*. Journal of Biomechanics, 2000. **33**: p. 1575-1583.
13. Van Rietbergen, B., H. Weinans, R. Huiskes, and A. Odgaard, *A new method to determine trabecular bone elastic properties and loading using micromechanical finite element models*. Journal of Biomechanics, 1995. **28**(1): p. 69-81.
14. Stölken, J.S., and Kinney, J.H., *On the importance of geometric nonlinearity in finite-element simulations of trabecular bone failure*. Bone, 2003. **33**(4): p. 494-504.
15. Bayraktar, H.H., M.F. Adams, A. Gupta, P. Papadopoulos, and T.M. Keaveny. *The role of large deformations in trabecular bone mechanical behavior*. in *ASME Bioengineering Conference*. 2003. Key Biscayne, FL.
16. Wachtel, E.F. and T.M. Keaveny, *Dependence of trabecular damage on mechanical strain*. Journal of Orthopaedic Research, 1997. **15**: p. 781-787.

17. Fyhrie, D.P. and M.B. Schaffler, *Failure mechanisms in human vertebral cancellous bone*. Bone, 1994. **15**(1): p. 105-9.
18. Bayraktar, H.H., A. Gupta, R.Y. Kwon, P. Papadopoulos, and T.M. Keaveny, *The Modified Super-Ellipsoid yield criterion for human trabecular bone*. Journal of Biomechanical Engineering, 2004. **126**: p. 677-684
19. Keaveny, T.M., *On Stolken and Kinney (Bone 2003;33(4): 494-504)*. Bone, 2004. **34**(5): p. 912-912.
20. Morgan, E.F. and T.M. Keaveny, *Dependence of yield strain of human trabecular bone on anatomic site*. Journal of Biomechanics, 2001. **34**(5): p. 569-577.
21. Beck, J.D., B.L. Canfield, S.M. Haddock, T.J.H. Chen, M. Kothari, and T.M. Keaveny, *Three-dimensional imaging of trabecular bone using the Computer Numerically Controlled Milling technique*. Bone, 1997. **21**: p. 281-287.
22. Niebur, G.L., J.C. Yuen, A.C. Hsia, and T.M. Keaveny, *Convergence behavior of high-resolution finite element models of trabecular bone*. Journal of Biomechanical Engineering, 1999. **121**(6): p. 629-635.
23. Hollister, S.J., J.M. Brennan, and N. Kikuchi, *A homogenization sampling procedure for calculating trabecular bone effective stiffness and tissue level stress*. Journal of Biomechanics, 1994. **27**(4): p. 433-444.
24. Papadopoulos, P. and J. Lu, *A general framework for the numerical solution of problems in finite elasto-plasticity*. Computer Methods in Applied Mechanics and Engineering, 1998. **159**(1-2): p. 1-18.
25. Papadopoulos, P., and Lu, J., *On the formulation and numerical solution of problems in anisotropic finite plasticity*. Computer Methods in Applied Mechanics and Engineering, 2001(190): p. 4889-4910.
26. Green, A.E. and P.M. Naghdi, *A general theory of an elastic-plastic continuum*. Arch Rat Mech Anal, 1965. **18**: p. 251-281.
27. Green, A.E. and P.M. Naghdi, *Some Remarks on Elastic-Plastic Deformation at Finite Strain*. International Journal of Engineering Science, 1971. **9**(12): p. 1219-&.
28. Bayraktar, H.H., E.F. Morgan, G.L. Niebur, G.E. Morris, E.K. Wong, and T.M. Keaveny, *Comparison of the elastic and yield properties of human femoral trabecular and cortical bone tissue*. J Biomech, 2004. **37**(1): p. 27-35.
29. Bayraktar, H.H., E.F. Morgan, G.L. Niebur, G. Morris, E.K. Wong, and T.M. Keaveny, *Comparison of the elastic and yield properties of human femoral trabecular and cortical bone tissue*. Journal of Biomechanics, 2003. **37**(1): p. 27-35.
30. Adams, M.F., Bayraktar, H.H., Keaveny, T.M., and Papadopoulos, P., *Ultrascalable implicit finite element analyses in solid mechanics with over a half a billion degrees of freedom*. ACM/IEEE Proceedings of SC2004: High Performance Networking and Computing, 2004.
31. Odgaard, A. and H.J. Gundersen, *Quantification of connectivity in cancellous bone, with special emphasis on 3-D reconstructions*. Bone, 1993. **14**(2): p. 173-82.
32. Hildebrand, T., A. Laib, R. Müller, J. Dequeker, and P. Rüegsegger, *Direct three-dimensional morphometric analysis of human cancellous bone: microstructural*

data from spine, femur, iliac crest, and calcaneus. Journal of Bone and Mineral Research, 1999. **14**(7): p. 1167-74.
33. Jaasma, M.J., H.H. Bayraktar, G.L. Niebur, and T.M. Keaveny, *Biomechanical effects of intraspecimen variations in tissue modulus for trabecular bone*. Journal of Biomechanics, 2002. **35**(2): p. 237-246.
34. van der Linden, J.C., D.H. Birkenhager-Frenkel, J.A. Verhaar, and H. Weinans, *Trabecular bone's mechanical properties are affected by its non-uniform mineral distribution*. J Biomech, 2001. **34**(12): p. 1573-80.
35. Crawford, R.P., C.E. Cann, and T.M. Keaveny, *Finite element models predict in vitro vertebral body compressive strength better than quantitative computed tomography*. Bone, 2003. **33**(4): p. 744-50.
36. Ün, K., G. Bevill, and T.M. Keaveny, *The Effects of Side-Artifacts on the Elastic Modulus of Trabecular Bone*. Journal of Biomechanics, 2006. **In Press**.
37. Van Rietbergen, B., D. Ulrich, W. Pistoia, R. Huiskes, and P. Ruegsegger. *Prediction of trabecular bone failure parameters using a tissue failure criterion.* in *Trans. Orthop. Res. Soc.* 1998. New Orleans.

Appendix A

To ensure that our reported trends for large-deformation failure mechanisms are numerically accurate, we performed a convergence study using 20 μm resolution images as compared to the coarsened 40 and 60 μm resolution meshes. Two high-density specimens from the femoral neck (BV/TV = 26.5% and 26.9%) and two low-density specimens from the vertebral body (BV/TV = 6.6% and 6.5%) were selected. Using small- and large-deformation finite element analyses, yield stress and the percent change in stress due large-deformation failure mechanisms (see Methods, Fig. 1) were compared between the 20 μm analyses and the coarsened models.

The percent change in strength due to large-deformation failure mechanisms changed by less than 1% for three of the specimens, but increased from 33% to 45% for one vertebral trabecular specimen (Fig. 2A). This change was due to the fact that the yield stress from the small-deformation analysis increased slightly relative to the coarsened model (1.3%), while the large deformation yield stress decreased by 5.7%. All other yield stresses changed by less than 1% between the 20 and 40-60 μm models. Based on these results, we conclude that the coarsened models can accurately capture yield stress, while small changes may occur for the change in strength for some low volume fraction specimens.

Tables

Table 1. Specimen and cadaver information. Asterisk (*) denotes specimens that were used in tissue material model calibration.

Anatomic Site	No. Specimens	No. Donors (male/female)	Age (years)	Volume Fraction
Femoral Neck*	11	10 (5/5)	66 ± 9	0.29 ± 0.05
Femoral Neck	10	10 (5/5)	72 ± 10	0.21 ± 0.05
Greater Trochanter	7	7 (5/2)	75 ± 9	0.11 ± 0.03
Proximal Tibia	7	5 (5/0)	62 ± 16	0.12 ± 0.03
Vertebral body	19	19 (4/15)	77 ± 11	0.10 ± 0.04

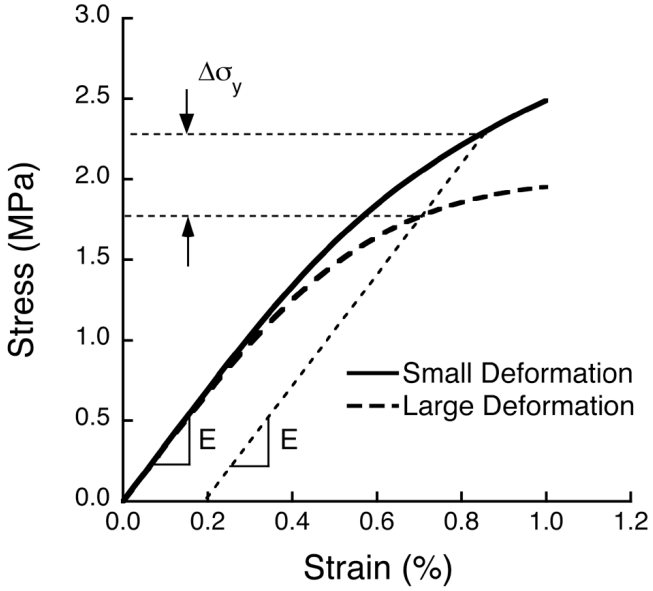

Fig. 1 Sample stress-strain curves from small- and large-deformation finite element analysis of a trabecular specimen typical of compressive loading. The yield point is defined using the 0.2% offset method (note that both curves have the same initial modulus). The change in strength due to large-deformation failure mechanisms is quantified as the percent difference in yield stress between the two (relative to the large deformation model).

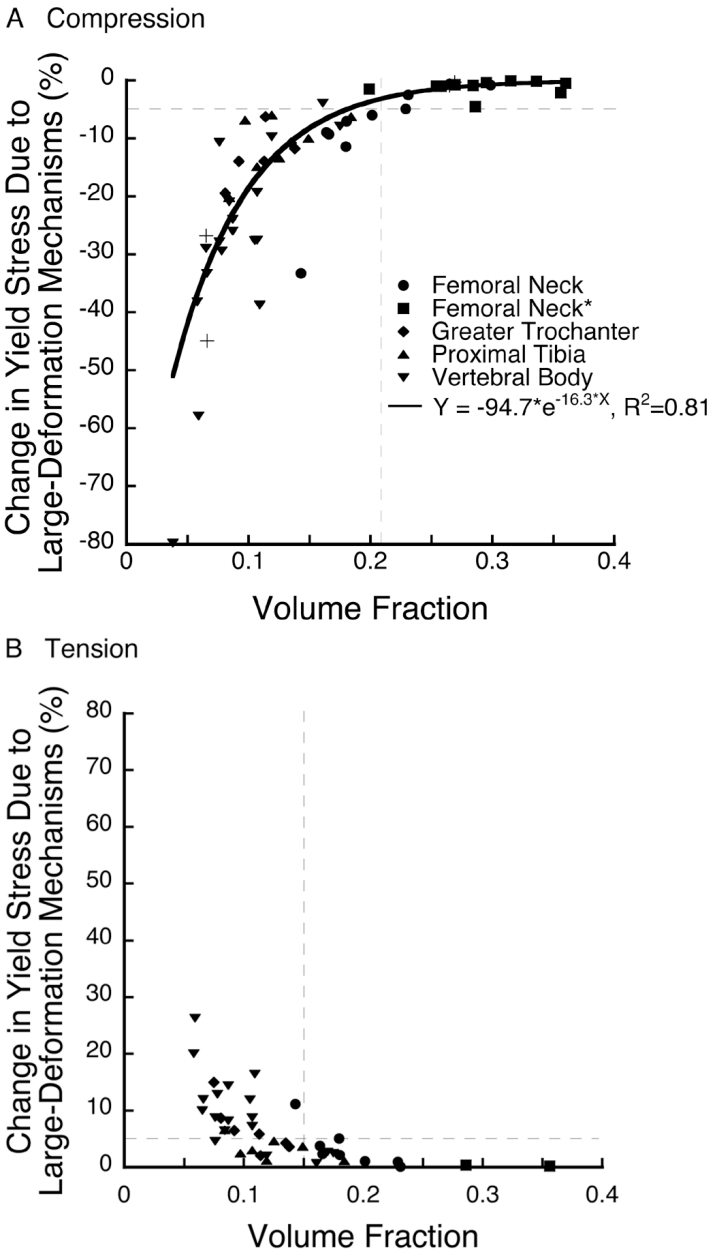

Fig 2. Change in strength due to large-deformation failure mechanisms plotted as a function of bone volume fraction for (A) compressive loading and (B) tensile loading. Specimens marked by a plus (+) symbol were analyzed at 20 μm resolution (see Appendix A). Horizontal dashed lines show 5% large-deformation effects at yield, and vertical dashed lines denote the corresponding threshold volume fraction.

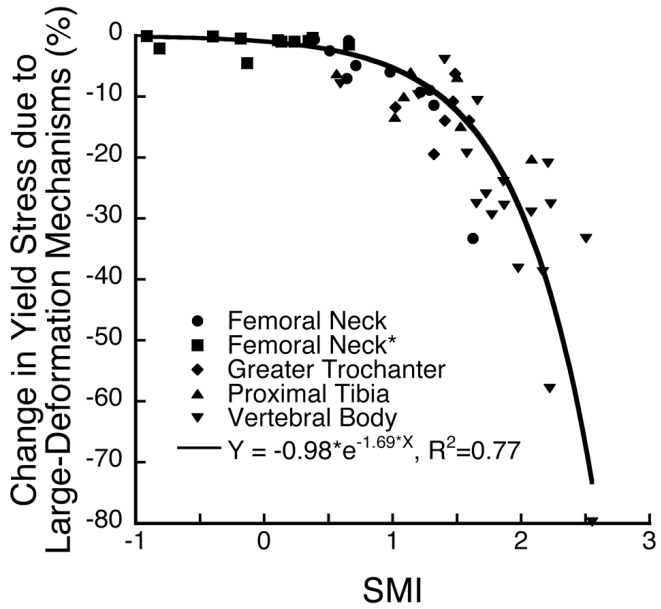

Fig 3. The percent change in strength correlated well with structure model index (SMI), indicating that the mechanism behind these large-deformation failure mechanisms is the transition from plate-like structure in trabeculae (SMI = 0) to a more rod-like structure (SMI = 3).

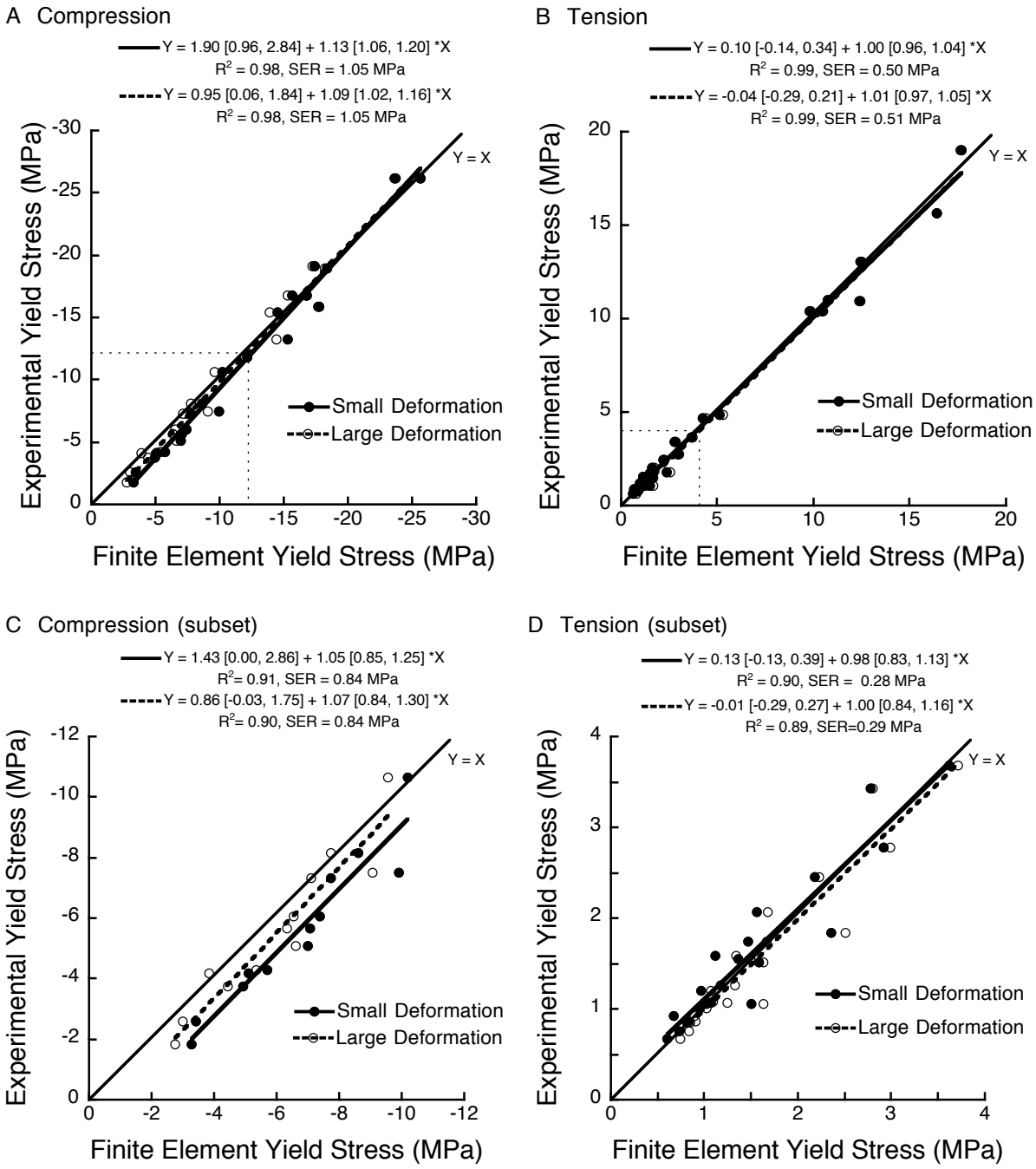

Fig. 4 Experimental measurement and finite element predictions of yield stress for (A) compressive and (B) tensile loading. The regression for each loading mode was repeated for the subset of specimens with bone volume fractions less than the critical values (denoted by dashed lines in A, B) for (C) compressive (n=12) and (D) tensile (n=18) loading. Mean errors for the finite element predictions of yield (relative to the ideal Y=X) are shown in Figure 5. Values in brackets ([ ]) represent 95% confidence intervals for the slope and intercept. SER – standard error of the regression.

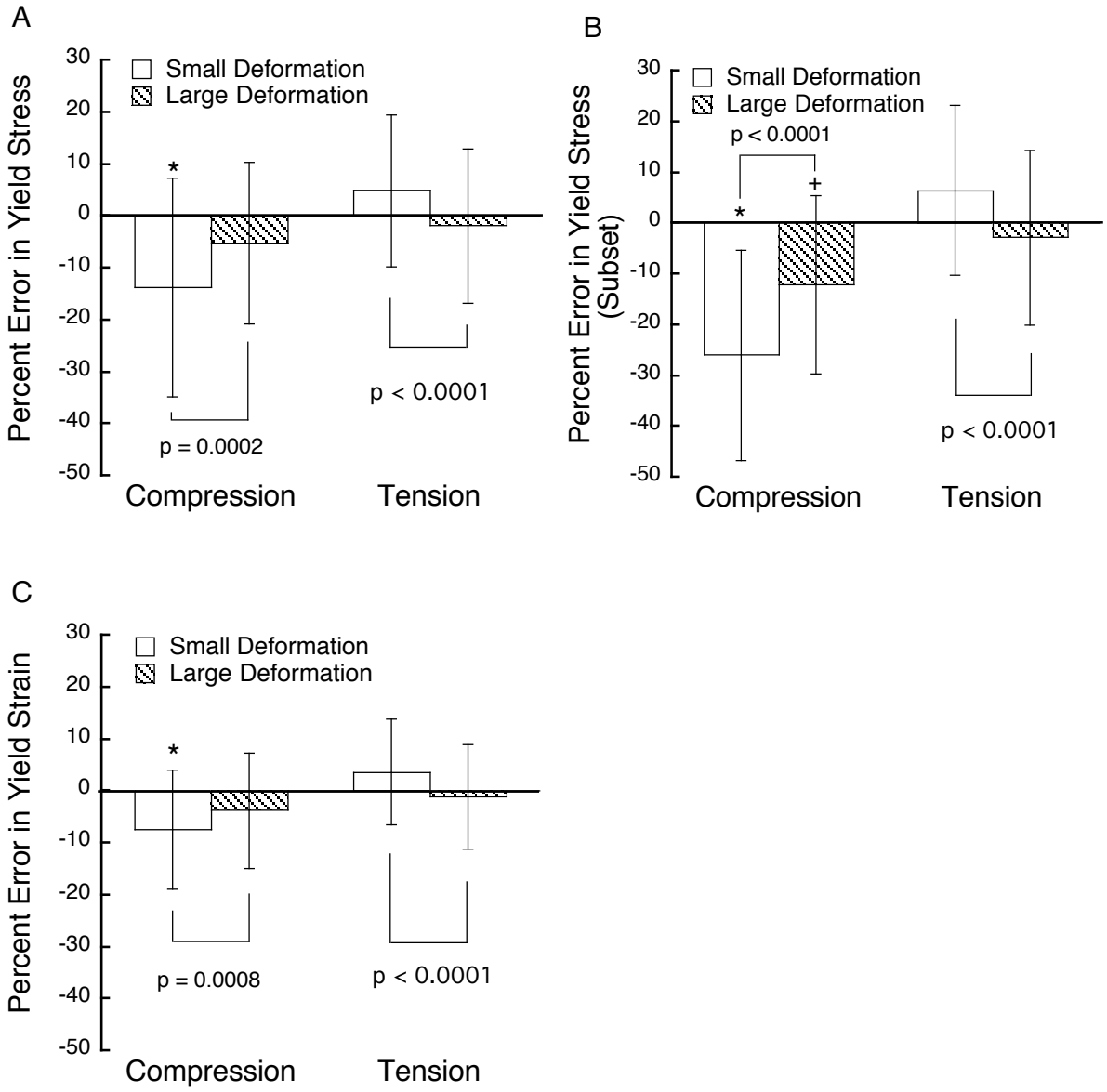

Fig. 5 Mean arithmetic error between finite element predictions and experimental measurements of yield for small- versus large-deformation analysis. Errors are given for (A) yield stress (corresponding to Figures 4A, 4B), (B) yield stress (corresponding to the subset of specimens in Figures 4C, 4D), and (C) yield strain (complete data set). Error bars represent one standard deviation. Note: all data are paired. (*: $p < 0.006$, +: $p = 0.04$ vs. zero).